The EMBO Journal Vol. 20 No. 15 pp. 4041–4054, 2001

Mammalian Golgi-associated Bicaudal-D2 functions in the dynein–dynactin pathway by interacting with these complexes

Casper C.Hoogenraad[1,2], Anna Akhmanova[1], Steven A.Howell[3], Bjorn R.Dortland[1], Chris I.De Zeeuw[2], Rob Willemsen[1], Pim Visser[1], Frank Grosveld[1] and Niels Galjart[1,4]

[1]MGC Departments of Cell Biology and Genetics and [2]Department of Anatomy, Erasmus University, PO Box 1738, 3000 DR Rotterdam, The Netherlands and [3]Laboratory of Protein Structure, National Institute for Medical Research, The Ridgeway, London NW7 1AA, UK

[4]Corresponding author
e-mail: galjart@ch1.fgg.eur.nl

C.C.Hoogenraad and A.Akhmanova contributed equally to this work

Genetic analysis in *Drosophila* suggests that Bicaudal-D functions in an essential microtubule-based transport pathway, together with cytoplasmic dynein and dynactin. However, the molecular mechanism underlying interactions of these proteins has remained elusive. We show here that a mammalian homologue of Bicaudal-D, BICD2, binds to the dynamitin subunit of dynactin. This interaction is confirmed by mass spectrometry, immunoprecipitation studies and *in vitro* binding assays. In interphase cells, BICD2 mainly localizes to the Golgi complex and has properties of a peripheral coat protein, yet it also co-localizes with dynactin at microtubule plus ends. Overexpression studies using green fluorescent protein-tagged forms of BICD2 verify its intracellular distribution and co-localization with dynactin, and indicate that the C-terminus of BICD2 is responsible for Golgi targeting. Overexpression of the N-terminal domain of BICD2 disrupts minus-end-directed organelle distribution and this portion of BICD2 co-precipitates with cytoplasmic dynein. Nocodazole treatment of cells results in an extensive BICD2–dynactin–dynein co-localization. Taken together, these data suggest that mammalian BICD2 plays a role in the dynein–dynactin interaction on the surface of membranous organelles, by associating with these complexes.

Keywords: Bicaudal-D/dynactin/dynein/Golgi/vesicular transport

Introduction

The product of the *Drosophila melanogaster Bicaudal-D* gene, Bic-D, is a cytoplasmic, α-helical coiled-coil protein (Suter *et al*., 1989; Wharton and Struhl, 1989), which is highly conserved from *Caenorhabditis elegans* to man and has two homologues in mammals, BICD1 (Baens and Marynen, 1997) and BICD2 (KIAA0699). In *D.melanogaster*, *Bic-D* is essential for the establishment of oocyte identity, as well as for the determination of the oocyte anterior–posterior axis and its dorsal–ventral polarity (Suter *et al*., 1989; Wharton and Struhl, 1989; Suter and Steward, 1991; Swan and Suter, 1996). Mutations in *Bic-D* disrupt the proper accumulation and distribution of factors important for oocyte differentiation and patterning, and affect the organization and polarization of the microtubule network during oogenesis (Suter *et al*., 1989; Theurkauf *et al*., 1993; Mach and Lehmann, 1997). Based on genetic data and the localization of Bic-D protein, it has been suggested that it constitutes a part of the microtubule-dependent mRNA transport or anchoring mechanism (Swan and Suter, 1996; Mach and Lehmann, 1997; Swan *et al*., 1999).

One of the major components of the intracellular transport machinery is cytoplasmic dynein, a minus-end-directed, microtubule-based motor. It is a large protein complex, which requires the activity of another multisubunit complex, dynactin, for most of its known cellular functions (for review see Karki and Holzbaur, 1999). Dynactin consists of two structural domains: an actin-like backbone, thought to be responsible for cargo attachment, and a projecting shoulder–sidearm that interacts with cytoplasmic dynein as well as with microtubules. The shoulder–sidearm complex contains p150^{Glued}, dynamitin (p50) and p24 subunits, while the actin-like backbone contains Arp1, CapZ, p62, Arp11, p27 and p25 (Eckley *et al*., 1999). Genetic analysis in *D.melanogaster* suggests that Bic-D functions in a transport pathway that involves cytoplasmic dynein and dynactin (Swan *et al*., 1999). This is in line with the fact that the distribution of Bic-D at different stages of oogenesis resembles the localization of the minus ends of microtubules (Mach and Lehmann, 1997) and of cytoplasmic dynein and dynactin (Li *et al*., 1994; McGrail *et al*., 1995). Bic-D has been shown to interact with the *Egalitarian* gene product (Mach and Lehmann, 1997). In addition, yeast two-hybrid analysis has suggested an association of Bic-D with lamin Dm0 (Stuurman *et al*., 1999). How these interactions relate to the proposed role of Bic-D and how Bic-D acts in the dynein–dynactin pathway are currently unclear.

Recently, we isolated mouse BICD2 in a yeast two-hybrid screen, using the microtubule binding protein CLIP-115 as bait (C.Hoogenraad, A.Akhmanova, F.Grosveld and N.Galjart, in preparation). These data suggest that, similar to *D.melanogaster* Bic-D, BICD2 could also be involved in microtubule-dependent transport. Here we demonstrate an interaction between mammalian BICD2 and the dynein–dynactin complexes, and we show that BICD2 associates with membranous organelles. We propose that BICD proteins play a direct role in dynein-mediated transport and that this function is conserved from *D.melanogaster* to mammals.

© European Molecular Biology Organization

Results

Association of BICD2 with dynein and dynactin

Mammalian BICD2 is a coiled-coil protein, which, like *D.melanogaster* Bic-D (Stuurman *et al*., 1999), contains three segments with multiple heptad repeats (Figure 1A). The C-terminal segment 3 shows the highest degree of evolutionary conservation (Figure 1A). In order to characterize BICD2, we generated polyclonal antibodies against the N-terminal part of BICD2 [glutathione *S*-transferase (GST)–NBICD2; antiserum #2293], as well as antibodies against the C-terminal coiled-coil segment of the protein (GST–CBICD2; antiserum #2298; see Figure 1A). In COS-1 cell lysates, both antisera specifically recognize proteins of ~98 kDa, which correlates with the expected size of BICD2 (Figure 1B). In BICD2-transfected cells, the intensity of the signal at the 98 kDa position increases, confirming that it represents BICD2, while antibodies, pre-incubated with their corresponding antigens, display no reaction on western blots (Figure 1B). Thus, the #2293 and #2298 antibodies specifically recognize BICD2 in COS-1 cells.

Fractionation of COS-1 cell lysates by high-speed centrifugation suggests that BICD2 is associated with membranous organelles, as part of the endogenous BICD2 protein is present in the pellet in the absence of detergent, while in the presence of 1% Triton X-100 all BICD2 immunoreactivity is recovered in the supernatant (Figure 1C). In the presence of detergent, both antisera are able to immunoprecipitate BICD2 from total extracts of COS-1 and HeLa cells (Figure 1D and E and data not shown). Coomassie Blue staining of a large scale immunoprecipitation from HeLa cells with antiserum #2298 revealed that these antibodies precipitate two major proteins with an apparent molecular mass of 97–100 kDa, in addition to several other proteins, ranging in size from >200 to 130 kDa (Figure 1D). Mass spectrometry on excised gel slices identified the 97–100 kDa bands as BICD2 isoforms, while other proteins, co-precipitating with the #2298 antiserum, were shown to be dynein heavy chain, non-muscle myosin IIA, p150^{Glued} and leucine-rich protein (Figure 1D, Table I; proteins smaller than ~80 kDa could not be identified because of IgG contamination). Here we focus on the interaction between BICD2 and dynein–dynactin.

To verify the results of mass spectrometry, immunoprecipitates obtained with anti-BICD2 antibodies #2298 and #2293 were analysed by western blotting. This revealed that both antisera bring down cytoplasmic dynein, as detected with an anti-dynein intermediate chain (DIC) antibody, and dynactin, as detected with anti-p150^{Glued} and anti-Arp1 antibodies (Figure 1E). These co-precipitations are specific, as #2293 pre-immune serum does not bring down dynein–dynactin or BICD2, and as none of the antisera co-precipitate CLIP-170, a cytosolic, microtubule-associated protein (Figure 1E). Furthermore, in a reciprocal experiment, antibodies against DIC, p150^{Glued} and Arp1 co-precipitate BICD2 (Figure 1F). Thus, dynein and dynactin can be co-immunoprecipitated with BICD2 antisera and vice versa. As a substantial co-immunoprecipitation of dynein and dynactin, using specific antisera against components of these complexes, has not been observed (Gill *et al*., 1991), it seems unlikely that the interaction of BICD2 with dynein occurs through dynactin, or vice versa.

Yeast two-hybrid interactions of BICD2

Structural studies have shown that *D.melanogaster* Bic-D forms dimers, which might fold up further via an intramolecular interaction of coiled-coil segments 2 and 3 (Stuurman *et al*., 1999). To test whether mammalian BICD2 interacts with itself and with components of the dynactin complex, we set up a yeast two-hybrid assay, using each of the three coiled-coil segments of BICD2 as separate fusion proteins, either linked to the DNA binding domain (BD), or to the activation domain (AD) of GAL4 (Figure 2A). As fusions of coiled-coil segments 1 and 3 to the GAL4 DNA-BD already strongly activated transcription of the reporter gene in the absence of GAL4 AD fusions, these clones were not used further. The GAL4 DNA-BD fusions of segment 2 and of the C-terminal part of segment 3 (amino acids 706–810) did not activate transcription by themselves and could be used to test a putative self-association of BICD2 (Figure 2B). This analysis shows that segment 2 (BICD2B) interacts with itself, but not with other segments, while the C-terminal part of segment 3 (BICD2D) interacts with itself, with the complete segment 3 (BICD2C) and with segment 1 (BICD2A; Figure 2B). The lack of interaction between BICD2B and -D is somewhat unexpected, given the proposal that Bic-D dimers fold up via segments 2 and 3 (Stuurman *et al*., 1999). Instead, we find that BICD2A and -D do associate; indicating that segments 1 and 3 might interact. However, it is possible that, *in vivo*, both associations (segment 1 with 3 and segment 2 with 3) occur. Such associations may serve as a mechanism for multimerization of BICD proteins and/or the regulation of interactions with other proteins.

We next examined the interaction of BICD2 fragments with all coiled-coil containing components of the dynactin complex, including p24, dynamitin and three adjacent p150^{Glued} fragments, as well as with the dynactin subunit Arp1 (Figure 2C). BICD2 does not associate with p150^{Glued}, p24, Arp1 or the control tropomyosin. Interestingly, coiled-coil segment 3 of BICD2 does interact with dynamitin, the C-terminal portion of this fragment (residues 706–810) being sufficient for the association. The other BICD2 fragments do not interact with dynamitin, suggesting that the association of the C-terminal domain is specific (Figure 2C). The direct nature of the BICD2–dynamitin interaction was confirmed by pull-down experiments, in which *in vitro* transcribed and translated BICD2 is retained by bacterially produced dynamitin (GST–p50), while myc- and green fluorescent protein (GFP)-tagged dynamitin (myc–GFP–p50) is retained by GST–CBICD2 (Figure 3A and B).

To demonstrate that BICD2 associates with dynamitin in transfected cells, we performed immunoprecipitations from extracts of COS-1 cells, overexpressing BICD2 (or GFP–BICD2$^{706–810}$) and myc–GFP–p50. We found that dynamitin co-precipitates with BICD2 from co-transfected cells (Figure 3C and D), whereas, in a similar experiment, no significant co-precipitation was detected between overexpressed BICD2 (or GFP–BICD2$^{706–810}$) and p150^{Glued} (Figure 3E). These results together support the yeast two-hybrid and pull-down analyses, and point to a

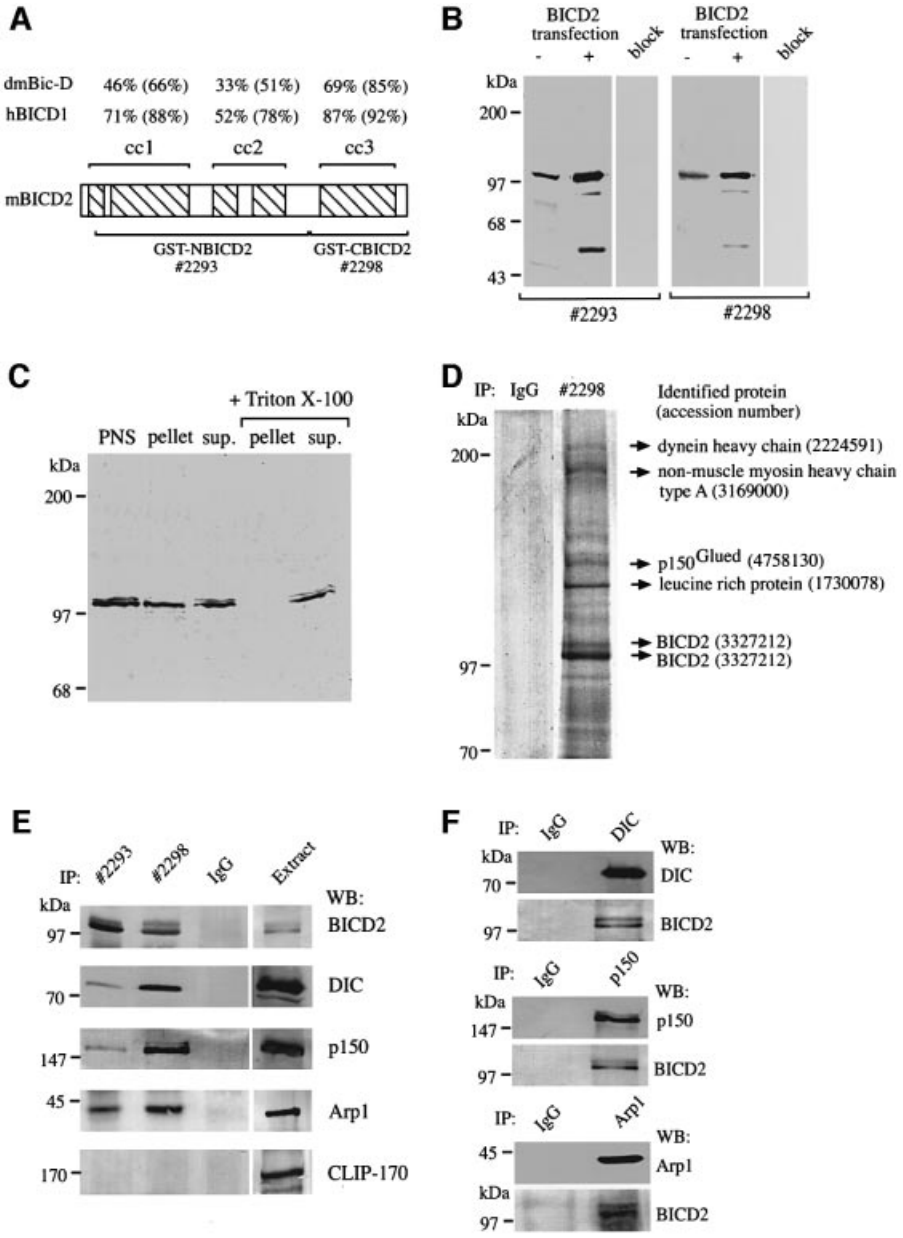

Fig. 1. Characterization of BICD2-specific antibodies. (**A**) Schematic representation of the domain structure of BICD2, which is characterized by five coiled-coil domains (hatched boxes) embedded in three segments (indicated above the diagram). The percentage of identity and (in parentheses) similarity between mouse BICD2 segments and those of human BICD1 (Baens and Marynen, 1997) or *D.melanogaster* Bic-D (accession No. P16568) is indicated. Antisera were directed against the N-terminal two segments of BICD2 (GST–NBICD2, antiserum #2293, amino acids 77–637) or the C-terminal segment (GST–CBICD2, antiserum #2298, amino acids 631–821). (**B**) Specificity of the BICD2 antibodies. Protein extracts, prepared from mock (–) or BICD2 (+) transfected COS-1 cells, were analysed by western blotting, using #2293 or #2298 antibodies, or antibodies pre-incubated with their corresponding antigens (lanes, marked 'block'). Approximately 5-fold less protein extract was loaded in the case of the BICD2 transfections, so that the signal in the transfected lanes was not too intense compared with the non-transfected samples. (**C**) Equal protein amounts of post-nuclear extracts (PNS), high-speed supernatant (sup.) and pellet fractions of COS-1 cells, incubated with or without 1% Triton X-100, were analysed by western blotting with antiserum #2293. (**D**) Coomassie Blue-stained 8% SDS–polyacrylamide gel of immunoprecipitates from HeLa cells, using anti-BICD2 antibody #2298 or pre-immune serum #2298 (IgG). The major protein bands were excised from the gel and subjected to mass spectrometry. Identified proteins, with their accession numbers, are shown on the right. Molecular weight markers are indicated. (**E**) Co-immunoprecipitation of cytoplasmic dynein and dynactin with BICD2 antisera. Lysates of HeLa cells were used for immunoprecipitation (IP) with anti-BICD2 antibodies #2293 and #2298, or pre-immune serum of #2293 (IgG). The precipitated proteins were resolved by SDS–PAGE and analysed by western blotting (WB) with antibodies against BICD2 (#2298), DIC, p150^{Glued} (p150), Arp1 and CLIP-170. Five per cent of the total extract used for immunoprecipitation was loaded as a control (BICD2 detection in the extract compared with the immunoprecipitate required five times longer exposure of the western blot; in all other cases, exposure times for immunoprecipitate and extract were the same). (**F**) Co-immunoprecipitation of BICD2 with cytoplasmic dynein and dynactin antibodies. Lysates of HeLa cells were used for immunoprecipitation (IP) with anti-DIC, anti-p150^{Glued} (p150) and anti-Arp1 antibodies, or with the #2293 pre-immune serum (IgG). Immunoprecipitates were analysed by western blotting (WB) with antibodies against BICD2 (#2298), DIC, p150^{Glued} (p150) and Arp1.

Table I. Mass spectrometry identification of BICD2-co-precipitating proteins

Protein	Number of matching peptides by MALDI and MS-FIT rank	Percent sequence coverage	Confirmation by nanospray (crosses indicate number of different MS^2 spectra obtained)
BICD2 lower band	12 (1)	17	not attempted
BICD2 upper band	40 (1)	43	++
Leucine-rich protein	32 (1)	34	+++
p150^{Glued}	17 (1)	14	+++
Non-muscle myosin heavy chain type A	39 (1)	24	not attempted
Dynein heavy chain	28 (1)	15	+++

direct and specific binding of BICD2 to dynamitin via the C-terminal part of BICD2.

BICD2 localizes to the Golgi complex and has properties of a peripheral coat protein

To analyse the subcellular localization of BICD2, we performed immunofluorescence experiments on cultured cells. Both with affinity-purified (Figure 4A) and full (Figure 4D1) antiserum #2293, a bright perinuclear and punctate cytoplasmic distribution of BICD2 is observed, which appears to concentrate around the microtubule organizing centre (MTOC). Labelling is abolished by pre-incubation of the antiserum with its antigen GST–NBICD2 (Figure 4B), but not with the GST–CBICD2 fusion (data not shown). Antiserum #2298 produces a very similar labelling pattern to #2293, but the punctate cytoplasmic staining is more prominent with this antiserum (Figure 4C). Labelling by the #2298 antibodies is inhibited by pre-incubation with GST–CBICD2, but not by GST–NBICD2 (data not shown). These data suggest that the #2293 and #2298 antisera specifically recognize BICD2 in immunofluorescence studies.

The high-speed fractionation results (Figure 1C) indicated that BICD2 is associated with membranous organelles. Combined with the immunofluorescence data, this suggests that, in interphase cells, BICD2 is localized either to the Golgi apparatus, the endoplasmic reticulum (ER)-to-Golgi intermediate compartment (ERGIC), or to recycling endosomes, which show an MTOC-dependent distribution (Burkhardt *et al.*, 1997). To distinguish between these possibilities we carried out double-labelling experiments with specific markers of the different compartments. Both epifluorescence and confocal microscopy reveal that the BICD2-positive structures show little overlap with endosomes labelled with antibodies against the transferrin receptor (Figure 4D1–3 and H1–3), or with other endosomal markers such as EEA1 and Rab5 (data not shown). BICD2 distribution is also distinct from that of p115, which labels the ERGIC (Figure 4E1–3). In cells incubated at 15°C, proteins that recycle between the ER and Golgi, such as p115, redistribute partially to peripheral clusters (Nelson *et al.*, 1998). These p115-containing structures are clearly not labelled with anti-BICD2 antiserum (Figure 4F1–3), further suggesting that BICD2 is not associated with the ERGIC.

BICD2 distribution in COS-1 cells does largely overlap with that of γ-adaptin (Figure 4G1–3), a marker for clathrin-coated vesicles at the *trans*-Golgi network (TGN) (Robinson and Kreis, 1992). This conclusion is confirmed by confocal microscopy in HeLa cells, which shows substantial overlap (but not a complete co-localization) of

A yeast-two hybrid constructs

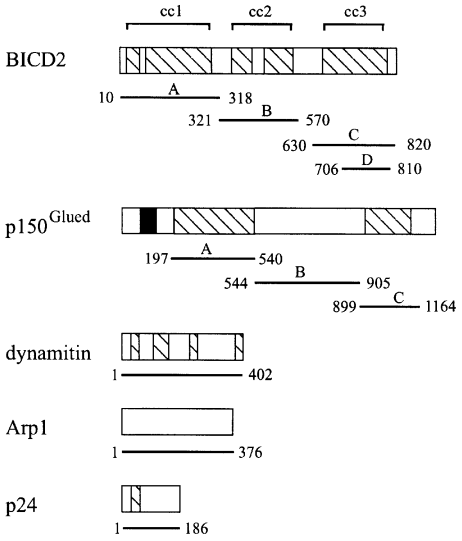

B

GAL4 DNA-BD fusion	GAL4 AD BICD2 A	B	C	D	tropo myosin
BICD2 B	–	++	–	–	–
BICD2 D	+	–	+	+	–

C

GAL4 DNA-BD fusion	GAL4 AD BICD2 A	B	C	D	tropo myosin
p150^{Glued}A	–	–	–	–	–
p150^{Glued}B	–	–	–	–	–
p150^{Glued}C	–	–	–	–	–
dynamitin	–	–	++	+	–
Arp1	–	–	–	–	–
p24	–	–	–	–	–

Fig. 2. Yeast two-hybrid interactions of BICD2. (**A**) Structure of the yeast two-hybrid constructs. The domain structure of BICD2, p150^{Glued}, dynamitin, Arp1 and p24, including coiled-coil regions (hatched boxes) and microtubule-binding motif (black box), are shown. The position of the protein fragments used in the yeast two-hybrid assay is indicated with horizontal lines below the respective diagrams. (**B** and **C**) Yeast two-hybrid analysis. Different segments of BICD2 were tested for BICD2 self-association (B), or for interaction with components of the dynactin complex (C). Protein segments were either fused to AD or DNA-BD of GAL4. The β-galactosidase activity in the yeast lysate is a measure of reporter gene activation. Enzymatic activity is expressed as (++), which indicates high activity (50–100 U); (+), which indicates moderate activity (5–50 U); and (–), which indicates low or no activity (0–5 U).

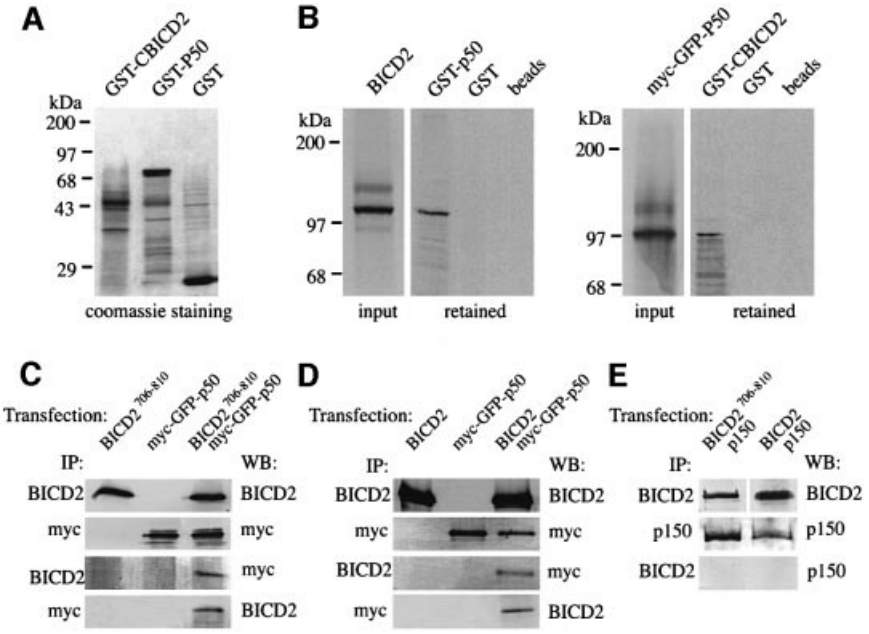

Fig. 3. Co-precipitation of dynamitin with BICD2. (**A**) Coomassie Blue-stained gel of purified bacterial fusion proteins (GST–CBICD2, GST–p50 and GST). Markers are indicated to the left. (**B**) *In vitro* interaction between BICD2 and p50 dynamitin. Radioactively labelled, *in vitro* transcribed and translated BICD2 (left panel, input lane) and myc- and GFP-tagged dynamitin (myc–GFP–p50, right panel, input lane) were incubated with the indicated, purified GST fusion proteins, or with glutathione beads only. Proteins, retained on the beads, were detected using SDS–PAGE and X-ray film exposure of dried gels. (**C**) Coiled-coil segment 3 of BICD2 co-precipitates with dynamitin. COS-1 cells were transfected with constructs expressing GFP–BICD2$^{706–810}$, myc–GFP–p50 or both proteins. Immunoprecipitations (IP) were performed using anti-BICD2 antibodies (#2298) or anti-myc antibodies. Western blots (WB) of the precipitated material were incubated with antibodies against myc, to detect dynamitin, or against BICD2 (#2298). (**D**) Full-length BICD2 co-precipitates with dynamitin. COS-1 cells were transfected with constructs expressing BICD2, myc–GFP–p50 or both proteins. IP were performed using anti-BICD2 antibodies (#2298) or anti-myc antibodies. WB of the precipitated material were incubated with antibodies against myc, to detect dynamitin, or against BICD2 (#2298). (**E**) BICD2 does not co-precipitate with p150^{Glued}. COS-1 cells were co-transfected with BICD2 (or GFP–BICD2$^{706–810}$) and p150^{Glued}, and protein homogenates were IP with anti-BICD2 (#2298) or anti-p150^{Glued} (p150) antibodies. WB of the IP material were incubated with anti-BICD2 antibodies (#2298) or with anti-p150^{Glued} (p150) antibodies. In (C–E), interactions between endogenous proteins are not detectable because ~8-fold less protein extract was used compared with (E) and (F) of Figure 1.

BICD2 and γ-adaptin (Figure 4I1–3). Incubation of cells at 20°C blocks vesicular transport from the TGN (Saraste and Kuismanen, 1984) and under these conditions the punctate cytoplasmic staining of BICD2 is no longer detectable (Figure 4J1). Instead, the protein accumulates in a region of the Golgi complex in close proximity to γ-adaptin (Figure 4J1–J3). These results suggest that the BICD2-labelled punctate structures, observed under normal growth conditions, could represent vesicles en route to (or from) the TGN.

Brefeldin A (BFA) is a fungal metabolite that interferes with ADP ribosylation factor-dependent vesicle budding in the secretory pathway (for review see Chardin and McCormick, 1999). After BFA treatment, p115 remains membrane bound (Nelson *et al*., 1998) (Figure 4K2), while peripheral coat proteins, such as β-COP and γ-adaptin, are released into the cytosol. A similar loss of BICD2 signal from Golgi membranes is observed within minutes after BFA treatment of COS-1 cells (Figure 4K1–3), indicating that BICD2 has properties of a cytosolic peripheral coat protein.

Immunoelectron microscopy was used to investigate further the subcellular distribution of BICD2. Ultrathin cryosections of COS-1 cells were incubated with rabbit antibodies #2293 against BICD2 and mouse antibodies against γ-adaptin, followed by incubation with secondary anti-rabbit and anti-mouse antibodies, conjugated with 6 and 10 nm colloidal gold, respectively (Figure 5). In all sections, a sparse but specific BICD2 labelling is observed, which is mainly located in the vicinity of the TGN, as identified by the γ-adaptin labelling (Figure 5A). In line with the high-speed fractionation results (Figure 1C), BICD2 appears to associate with membranes, as labelling is detected on tubular extensions (Figure 5C), at or near membrane stacks (Figure 5A and data not shown), as well as on budding and/or small cytoplasmic vesicles (Figure 5). Interestingly, the gold particles are often clustered (Figure 5A, B and D), suggesting that multiple BICD2 molecules might be present in a complex at the membrane.

Deletion analysis of BICD2 reveals Golgi targeting and dispersion domains

To determine how BICD2 is targeted to the Golgi, we fused full-length and truncated forms of BICD2 to GFP and studied their intracellular behaviour in transfection studies (Figures 6 and 7). At low expression levels, both full-length GFP–BICD2 and fusion proteins, containing the C-terminal coiled-coil part (GFP–BICD2$^{630–820}$ and GFP–BICD2$^{706–810}$), display a perinuclear accumulation, similar to endogenous BICD2. A strong overlap of GFP and anti-γ-adaptin antibody signal is detected (Figure 6A1–3 and C1–3), while little co-localization with the transferrin receptor is seen (Figure 6B1–3 and D1–3). Interestingly, in cells that overexpress GFP–BICD2$^{706–810}$, almost no endogenous BICD2 is detected in the Golgi apparatus (Figure 6E1–3, labelling

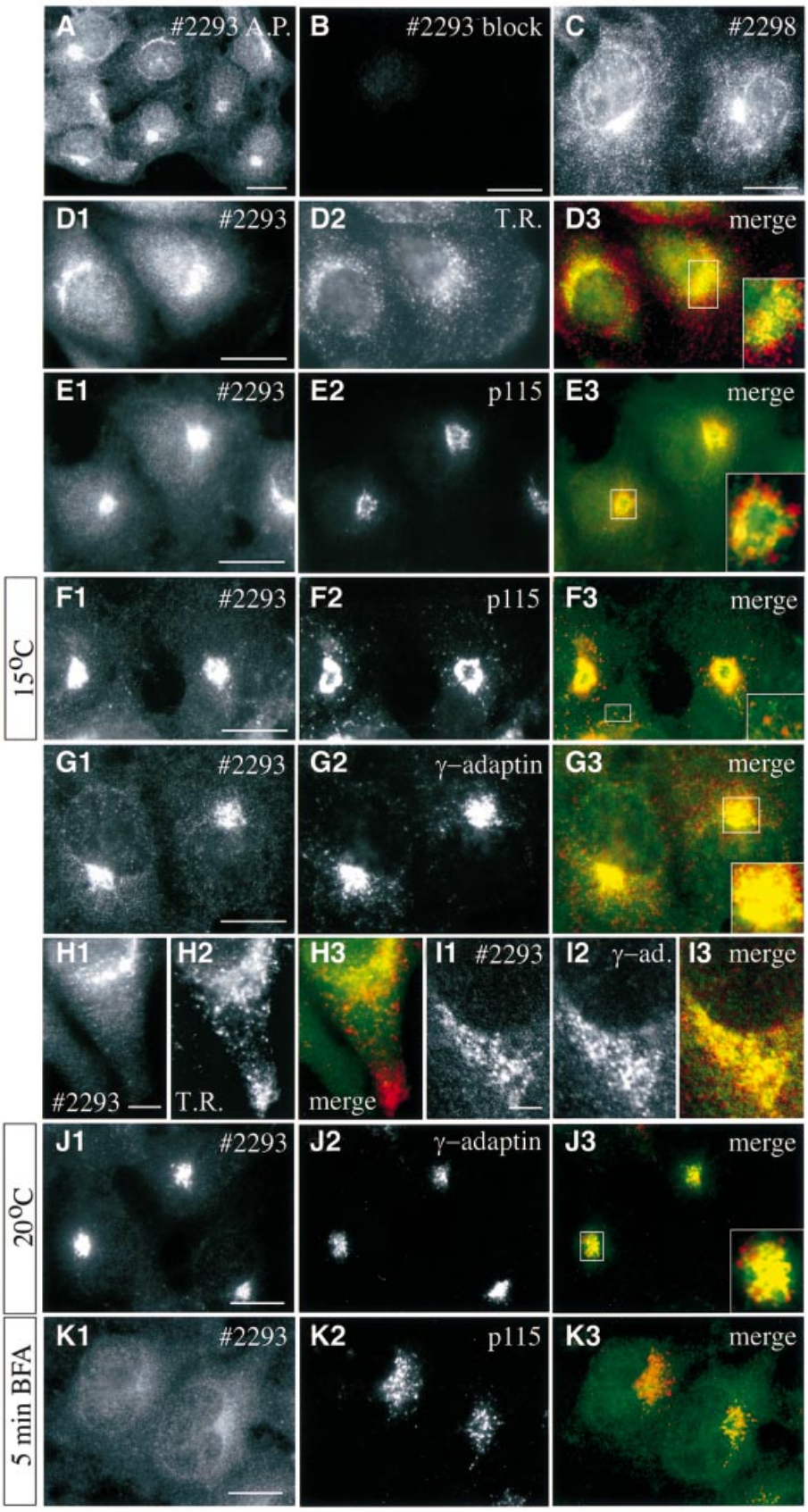
A
#2293 A.P.
B
#2293 block
C
#2298
D1
#2293
D2
T.R.
D3
merge
E1
#2293
E2
p115
E3
merge
15°C
F1
#2293
F2
p115
F3
merge
G1
#2293
G2
γ–adaptin
G3
merge
H1
#2293
H2
T.R.
H3
merge
I1
#2293
I2
γ–ad.
I3
merge
20°C
J1
#2293
J2
γ–adaptin
J3
merge
5 min BFA
K1
#2293
K2
p115
K3
merge

with antiserum #2293 against the N-terminus of BICD2). Nevertheless the Golgi remains in place and other resident proteins are detectable (Figure 6C2 and E3). These data indicate that the third coiled-coil segment of BICD2 contains a Golgi-targeting signal and that this fragment can compete with endogenous BICD2 for binding sites at the Golgi complex.

In contrast to the behaviour of the C-terminal BICD2 fusions, GFP proteins containing only the N-terminal or the middle part of BICD2 display a diffuse cytoplasmic staining (Figure 7A, B1 and C1). Surprisingly, overexpression of these proteins profoundly affects the organization of the Golgi apparatus (Figure 7B2). Deletion analysis reveals that fragmentation of the Golgi is dependent on amino acid residues 1–271 of BICD2, in which segment 1 is embedded (Figure 7A). As cells overexpressing full-length BICD2 (with or without a GFP tag, see Figures 6 and 8, respectively) show no apparent Golgi abnormalities, these data suggest that amino acids 1–271 perturb Golgi organization only when uncoupled from the remainder of BICD2.

Fragmentation of the Golgi apparatus is a characteristic feature of cells in which cytoplasmic dynein function is inhibited. Both overexpression of dynamitin (or other subunits of dynactin) and knock out of the cytoplasmic dynein heavy chain cause inhibition of dynein function (Burkhardt *et al*., 1997; Harada *et al*., 1998; Quintyne *et al*., 1999). In such cells, the distribution of endosomes and lysosomes is also altered. We therefore analysed whether overexpression of the N-terminal BICD2 segment causes a redistribution of transferrin receptor-positive endosomes, and found this to be the case (Figure 7C2). These data suggest that the N-terminal segment of BICD2 perturbs dynein-based motile events. To test whether the BICD2 N-terminus and dynein interact, we investigated co-precipitation of the DIC with selected GFP–BICD2 mutants in lysates of transfected COS-1 cells (Figure 7D). The results of these experiments indicate that every

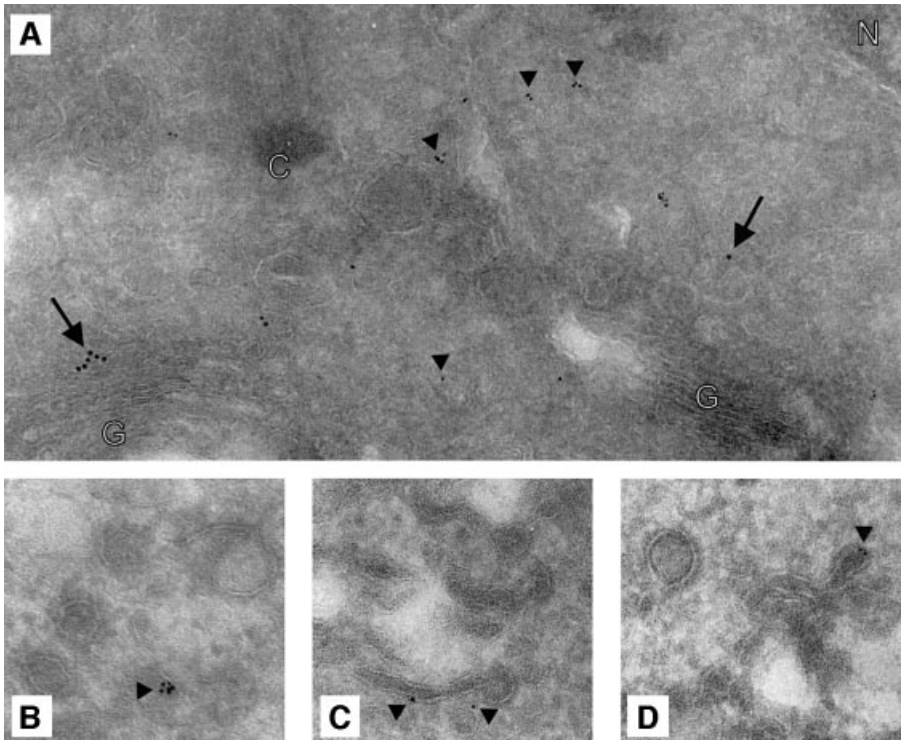

Fig. 5. Ultrastructural distribution of BICD2. (**A** and **B**) Ultrathin cryosections of COS-1 cells were immunolabelled with rabbit antiserum #2293 and mouse anti-γ-adaptin antibodies, followed by anti-rabbit and anti-mouse secondary antibodies, conjugated with 6 and 10 nm gold particles, respectively. Examples of BICD2 (arrowheads) and γ-adaptin (arrows) labelling are indicated. G, Golgi cisternae; C, centriole; N, nucleus. (**C** and **D**) Ultrathin cryosections were incubated with the #2293 antiserum only, followed by anti-rabbit secondary antibodies, conjugated with 6 nm gold. In (B, C and D), BICD2 labelling (arrowheads) of tubules and smooth vesicles in the proximity of the TGN is shown.

Fig. 4. Endogenous BICD2 distribution in COS-1 and HeLa cells. (A–C) COS-1 cells were fixed and processed for indirect immunofluorescence, using affinity purified (A.P.) #2293 anti-BICD2 antibodies (**A**), #2293 antibodies pre-incubated with GST–NBICD2 fusion protein (**B**) or #2298 anti-BICD2 antibodies (**C**). (D–K) Co-localization of BICD2 with different markers for membrane organelles. Each of the right-hand panels displays the merged signal of the left and middle images. The BICD2-specific (#2293) signal is shown in green and the corresponding marker in red. In some cases, a magnified view of the Golgi area is shown. Images were taken with an epifluorescence microscope, with the exception of H1-3 and I1-3, which were obtained with a confocal microscope. (**D** and **H**) HeLa cells, stained for BICD2 (D1, H1) and transferrin receptor (D2, H2). (**E**, **F** and **K**) COS-1 cells, stained for BICD2 (E1, F1, K1) and p115 (E2, F2, K2). Cells shown in F1-3 were cultured for 3 h at 15°C prior to fixation. Cells shown in K1-3 were incubated for 5 min in the presence of 5 μg/ml BFA. (**G** and **J**) COS-1 cells, stained for BICD2 (G1, J1) and γ-adaptin (G2, J2). Cells shown in J1-3 were incubated at 20°C for 3 h to block transport from the TGN. (**I**) HeLa cells stained for BICD2 (I1) and γ-adaptin (I2). Bars: 10 μm in (A–G), (J) and (K) and 5 μm in (H) and (I).

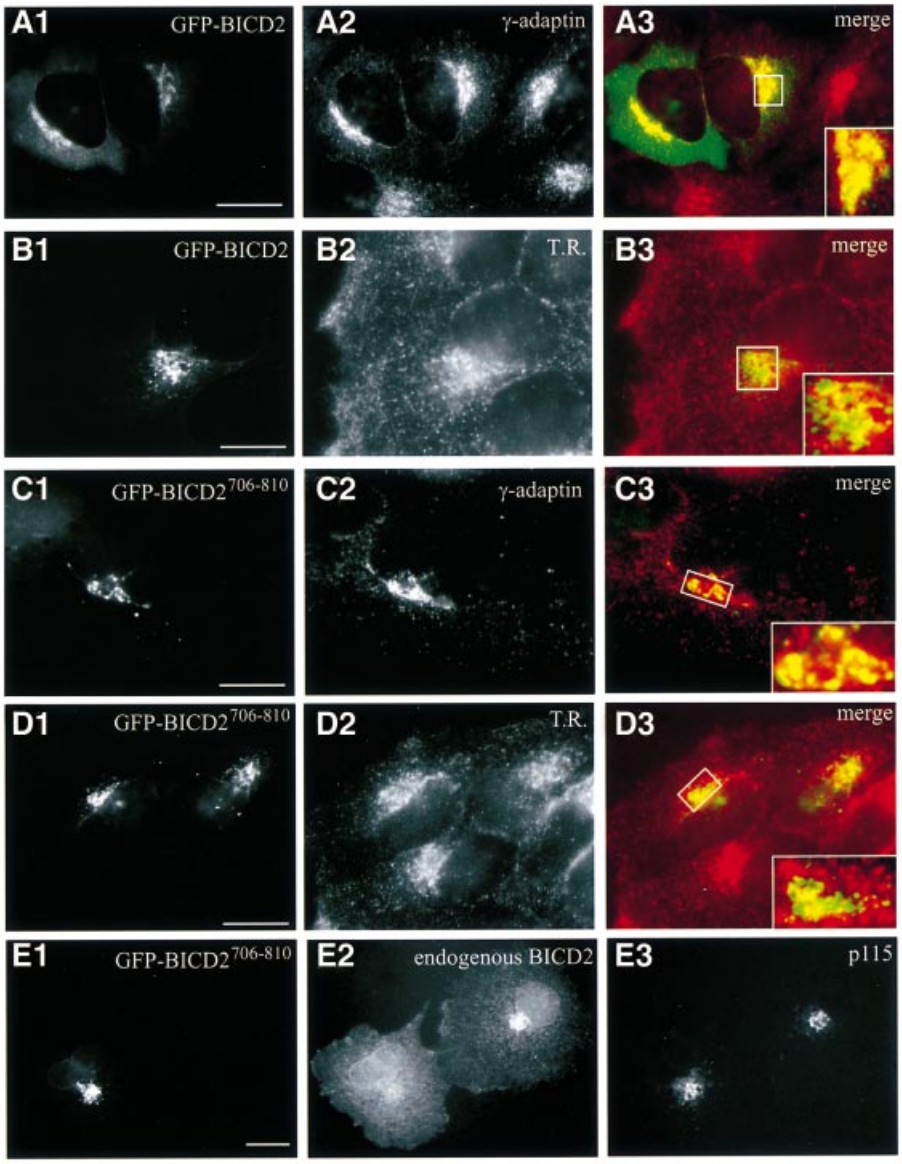

Fig. 6. C-terminal domain of BICD2 is responsible for Golgi localization. (A–D) HeLa cells were transfected with GFP–BICD2 (**A** and **B**) or GFP–BICD2$^{706–810}$ (**C** and **D**) and stained with antibodies against γ-adaptin (A2, C2) or transferrin receptor (B2, D2). Merged signal from GFP (green) and the organelle marker (shown in red) is shown on the right; a magnified view of the Golgi area is shown in the corner. (**E**) COS-1 cells were transfected with GFP–BICD2$^{706–810}$ and stained for endogenous BICD2 (#2293; E2) and p115 (E3). In the transfected cell, BICD2-specific staining in the Golgi area is strongly reduced compared with the neighbouring untransfected cell. Bars: 10 μm.

GFP–BICD2 construct, which includes amino acids 1–271, brings down the dynein complex, in line with an association between the N-teminus of BICD2 and dynein.

Co-localization of BICD2 and dynactin

As BICD2 interacts with dynamitin, we next investigated to what extent the intracellular distributions of these proteins overlap and how overexpression of these proteins affects their respective localization. In cells, expressing low levels of co-transfected myc–GFP–dynamitin and BICD2, prominent staining of the microtubule plus ends by GFP is detected (Figure 8A1 and B1). Accumulation of overexpressed BICD2 at the distal ends of microtubules is seen (Figure 8A2 and B2), which is enhanced compared with cells expressing low levels of BICD2 only (data not shown). Thus, overexpressed dynamitin and BICD2 co-localize to some extent. To investigate whether BICD2 co-localizes with dynactin in untransfected cells, Swiss 3T3 fibroblasts (Figure 8C–F) and COS-1 cells (data not shown) were stained with BICD2- and p150^{Glued}-specific antibodies. In these cells, some of the BICD2-positive, vesicle-like structures appear to assemble at those distal ends of microtubules which are also stained with anti-dynactin antibodies (Figure 8C and D). We next examined BICD2 distribution after a brief shift to room temperature, as this manipulation results in a significant co-localization of cytoplasmic dynein with dynactin, an association which is normally not observed (Vaughan *et al.*, 1999). Room temperature incubation leads to an increase in BICD2 and dynactin staining intensity at the microtubule plus ends, consistent with a direct association between BICD2 and dynactin (Figure 8E and F).

Co-localization of BICD2, dynactin and dynein in nocodazole-treated cells

Cultured cells treated with the tubulin sequestering compound nocodazole undergo microtubule depolymerization, resulting in inhibition of dynein-based motility and Golgi dispersal (Cole *et al*., 1996). We noted that in such cells both GFP–BICD2 (Figure 9A1) and endogenous BICD2 (Figure 9B1 and C1) are mainly present in cytoplasmic vesicular and/or aggregate-like structures. These do not co-localize significantly with any of the Golgi or endosomal markers described above (data not shown), but instead contain a considerable proportion of the cytoplasmic pool of p150^{Glued} and dynamitin (Figure 9A and B), as well as DIC (Figure 9C). Thus, nocodazole treatment of cultured cells surprisingly induces the coalescence of BICD2, dynactin and cytoplasmic dynein into structures of unknown composition. Interestingly, overexpression of the N-terminal part of BICD2 or dynamitin, which have similar disruptive effects on dynein-based organelle distribution in normal cultured cells, prevents the formation of these nocodazole-induced, cytoplasmic aggregates (Figure 9D and E), whereas the C-terminal portion of BICD2 (GFP–BICD2$^{706–810}$) co-localizes with endogenous BICD2 in the structures at low expression levels and inhibits their formation at high expression levels (data not shown). These data support the interaction between BICD2, dynactin and dynein, and suggest that the formation of complexes of these proteins in nocodazole-treated cells might be based on the same protein–protein interactions that are important for dynein-mediated motility.

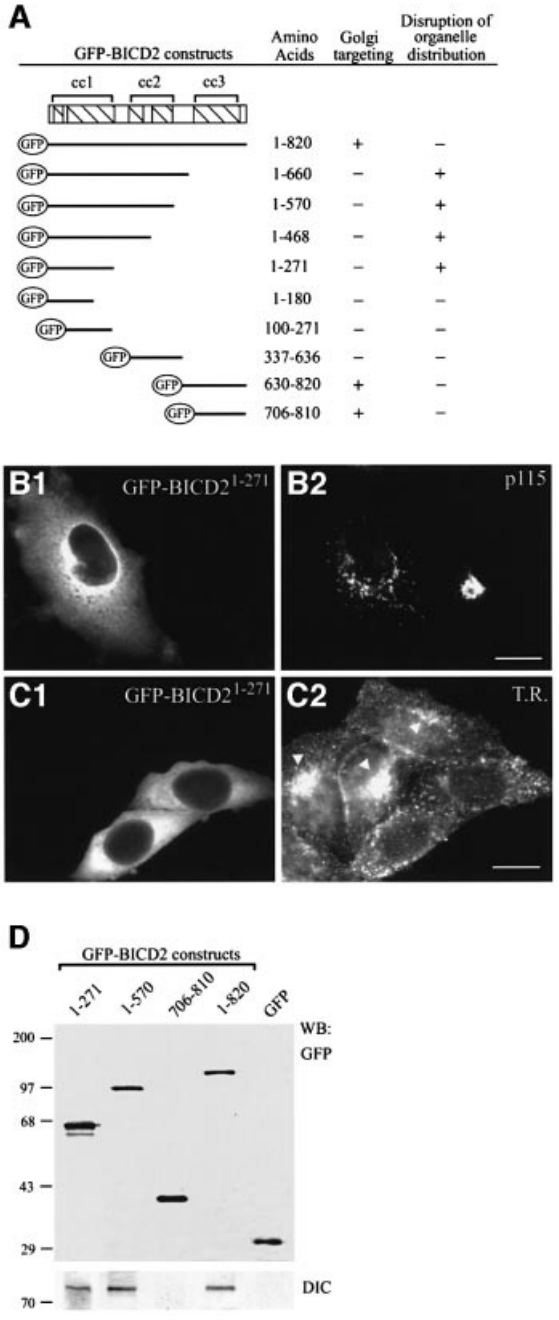

Discussion

The molecular mechanisms regulating cytoplasmic dynein-mediated motility are not completely understood, but it is becoming increasingly clear that they involve multiple protein–protein interactions and post-translational modifications. The dynactin complex, which can be linked to dynein through the interaction of its p150^{Glued} subunit with DIC (Vaughan and Vallee, 1995), might play a role in dynein–cargo binding, e.g. by associating with spectrin (Muresan *et al*., 2001), and might regulate the processivity of the dynein motor (King and Schroer, 2000). However, dynein itself can also bind to (and transport) various cargoes through its light and light intermediate chains (Tai *et al*., 1999; Young *et al*., 2000). We envisage a function for mammalian BICD2 in dynein-based transport that involves direct binding of BICD2 to the dynamitin subunit of dynactin and association with cytoplasmic dynein. These observations provide a molecular basis for the genetic evidence in *D.melanogaster*, which implicates Bic-D, dynein and dynactin functioning in a common pathway (Swan *et al*., 1999). Our findings suggest that the

Fig. 7. N-terminal domain of BICD2 co-precipitates with dynein and disrupts microtubule minus-end-directed organelle distribution. (**A**) Overview of GFP–BICD2 deletion constructs. COS-1 or HeLa cells were transfected with the indicated GFP–BICD2 fusion constructs, fixed and stained with Golgi- or endosome-specific antibodies, to analyse whether the transfected construct was targeted to the Golgi (+ indicates Golgi accumulation of the GFP fusion construct and – indicates absence of such accumulation) and whether organelle distribution was affected by the transfection (+ indicates a disrupted Golgi and endosome distribution, and – indicates a normal Golgi and endosome organization). (**B** and **C**) Organelle disruption by GFP–BICD2$^{1-271}$ overexpression. In (B), fragmentation of the Golgi complex is scored, as detected with anti-p115 antibodies (B2). In (C), a redistribution of endosomes to the periphery of the cell is scored, as detected by staining with antibodies against the transferrin receptor (C2). Organelle disruption is a robust phenotype; when present it occurs in all transfected cells, while neighbouring, non-transfected cells show a normal, compact perinuclear Golgi staining (B2) and prominent juxtanuclear accumulation of endosomes (indicated by arrowheads in C2). Bars: 10 μm. (**D**) Lysates of COS-1 cells, transfected with the indicated GFP proteins, were immunoprecipitated with monoclonal anti-GFP antibodies, and precipitated proteins were analysed by western blotting with polyclonal anti-GFP antibodies or with anti-DIC antibodies.

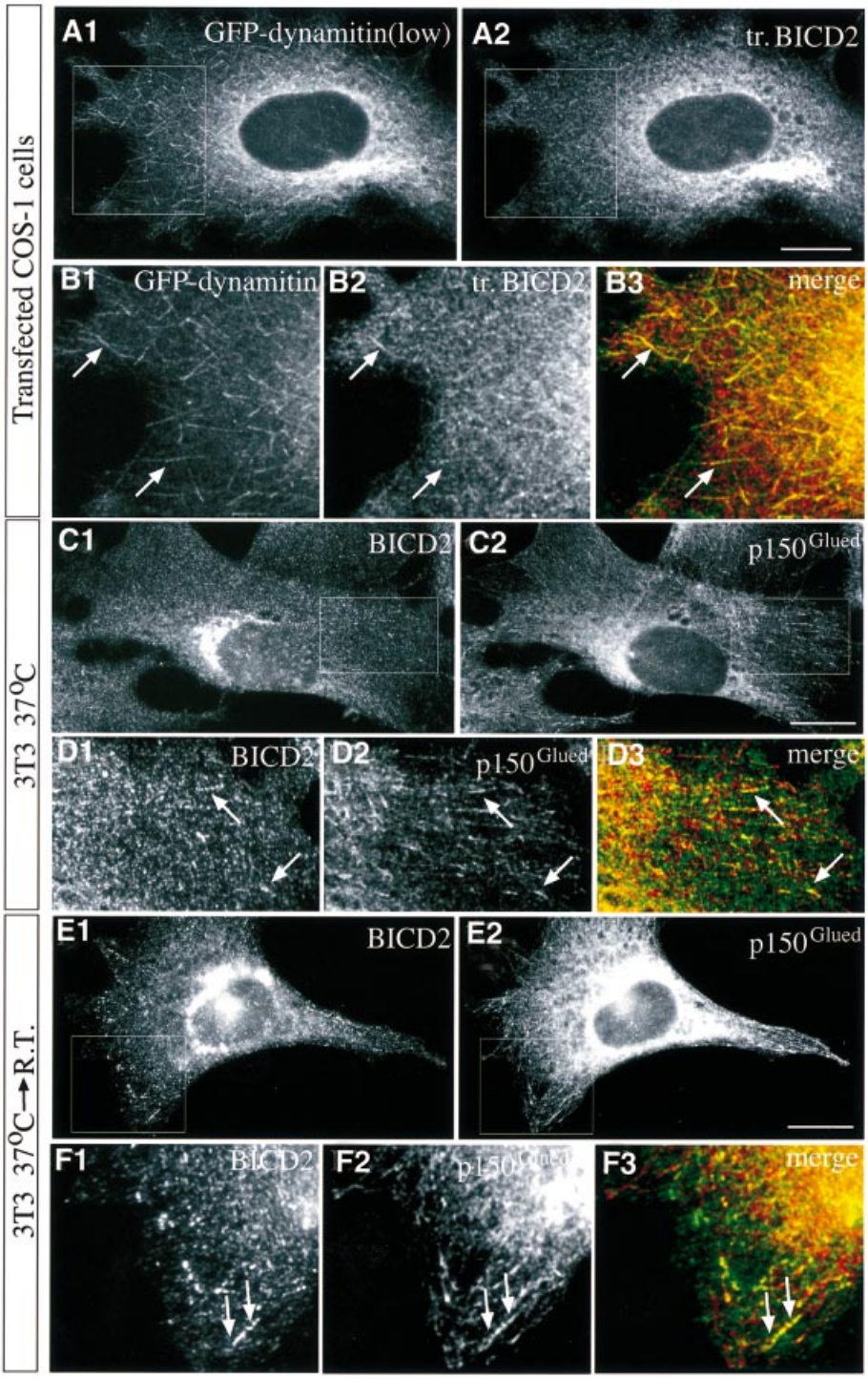

Fig. 8. Co-localization of BICD2 and dynactin components at microtubule distal ends. (**A** and **B**) COS-1 cells were co-transfected with myc–GFP–dynamitin and BICD2, and processed for immunofluorescence using anti-BICD2 antibodies #2293. GFP signal is shown in A1 and B1, while in A2 and B2 BICD2 is visualized. (B) A higher magnification view of the square, indicated in (A). B3 represents the merged image of B1 (green, GFP–dynamitin) and B2 (red, BICD2). Arrows indicate clear examples of co-localization of GFP–dynamitin and BICD2 at the distal ends of two microtubules. Bar: 10 μm. (**C**–**F**) Swiss 3T3 cells were stained with antibodies against BICD2 (C1, D1, E1, F1) and anti-p150^{Glued} (C2, D2, E2, F2). In D3 and F3, BICD2 (green) and p150^{Glued} (red) signals are merged. (D and F) Higher magnification views of the indicated parts in (C) and (E), respectively. Examples of co-localization of BICD2 and dynactin are indicated by arrows. In (E) and (F), cells were incubated at room temperature for 10 min prior to fixation. Bars: 10 μm.

BICD2 protein is a conserved component of the dynein–dynactin transport machinery.

BICD2 is a Golgi-associated protein, which could be part of the peripheral coat of particular membranes. Both the Golgi targeting of BICD2 and its binding to the dynamitin subunit of dynactin depend on coiled-coil segment 3. The relevance of these interactions is underscored by the fact that this is the most evolutionarily

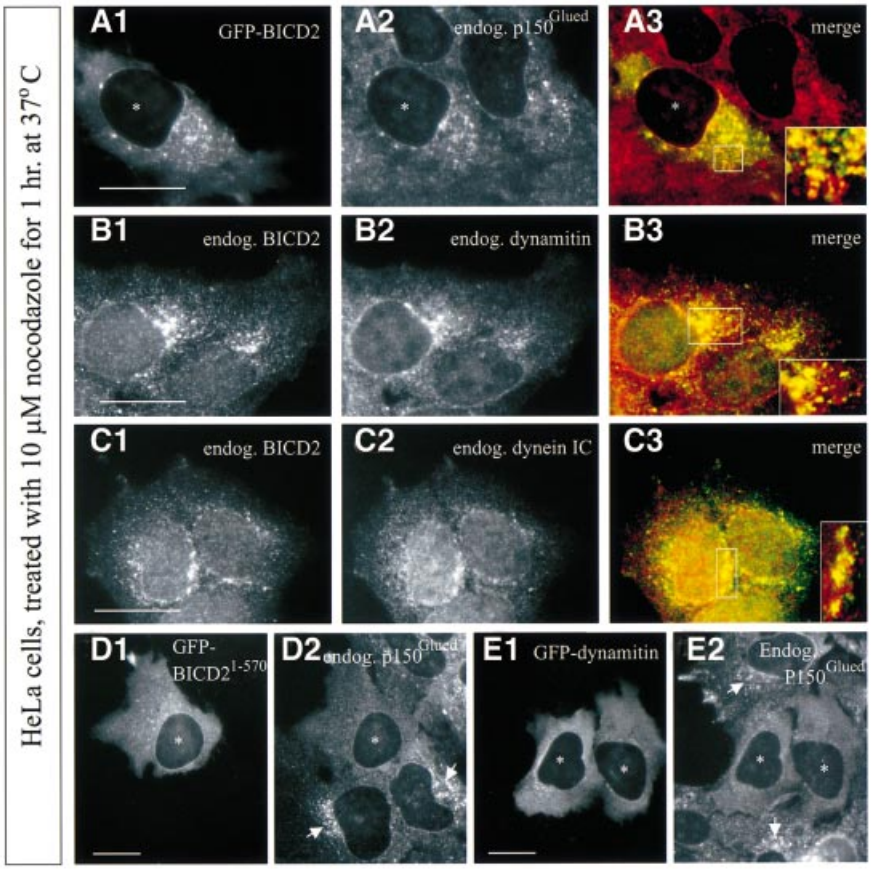

Fig. 9. Co-localization of BICD2 with dynactin and dynein components in nocodazole-treated cells. (A–E) HeLa cells, transfected with GFP–BICD2 (**A**), GFP–BICD2$^{1–570}$ (**D**), myc–GFP–dynamitin (**E**), or not transfected (**B**, **C**), were treated with 10 μM nocodazole for 1 h at 37°C prior to fixation, and processed for immunofluorescence with the indicated antibodies (endogenous signals). Asterisks mark the nuclei of transfected cells, and nocodazole-induced, dynactin-positive structures in untransfected cells are indicated by arrows. (A3–C3) are merged images (A1–C1 are in green; A2–C2 are in red). Higher magnification views of indicated areas are shown in the corner. Bars: 10 μm.

conserved part of the protein and the only *D.melanogaster* Bic-D segment indispensable for viability and proper localization during oogenesis (Oh *et al*., 2000; Oh and Steward, 2001). On the other hand, truncated BICD2 forms, which lack the third, but contain the first coiled-coil segment, can co-precipitate cytoplasmic dynein, suggesting that segment 1 can interact with a component of the dynein complex. Finally, overexpression of the N-terminal portion of BICD2 causes dispersion of cytoplasmic organelles and prevents the formation of nocodazole-induced, dynactin-positive aggregates, while overexpression of full-length BICD2 has none of these effects. To explain all these observations, we propose that soluble (excess, free) BICD2 folds up, for example, as a result of interaction of segments 1 and 3 (as observed in our yeast two-hybrid assay), or of segments 2 and 3 [as proposed in the structural analysis (Stuurman *et al*., 1999)]. Only when segment 3 engages in an interaction with one of its partners (dynamitin or a membrane-associated protein) do the other segments become available for interaction with other proteins (such as dynein components).

We hypothesize that when BICD2 is bound to a particular cargo through its C-terminus, it can stimulate the association of this cargo with dynein–dynactin through its N-terminus. If dynactin is the C-terminal cargo, then BICD2 might serve as a regulatory linker between dynein and dynactin. The role of BICD2 as such a linker is supported by the extensive co-localization of these protein complexes under conditions when dynein transport is inhibited by nocodazole treatment. Switching of BICD2 between different modes of interaction could regulate the affinity of the dynein–dynactin complex for (vesicular) cargo, or exercise a regulatory effect on dynein motor activity. A schematic representation of the putative conformations of BICD2 is shown in Figure 10.

In agreement with our hypothesis, we find co-localization of BICD2-positive, vesicular structures and dynactin at the distal ends of microtubules. The accumulation of dynactin and cytoplasmic dynein on microtubule plus ends was suggested to represent an early, cargo-loading stage of minus-end-directed organelle transport (Vaughan *et al*., 1999). In this view, BICD2-containing vesicles might be loaded on dynactin-carrying microtubule distal ends, in order to be transported along microtubules. One possibility is that BICD2 interacts with dynactin and the peripheral coat of membrane organelles simultaneously. This could be a result of multimerization of BICD2 proteins on the membrane surface or through unfolding of the last coiled-coil segment within one BICD2 dimer. Whatever the actual mechanism, all models predict that overexpression of the C-terminal segment of BICD2 by itself should have a dominant-negative effect on BICD2 function.

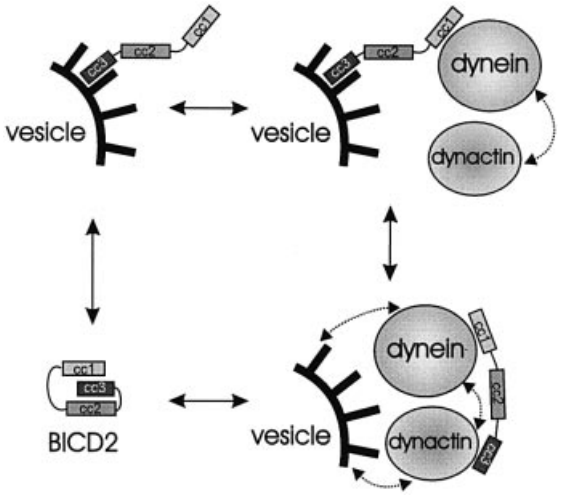

Fig. 10. Schematic representation of the possible conformations and interactions of BICD2. The BICD2 homodimer is represented by three boxes, corresponding to the three coiled-coil segments (cc1,cc2 and cc3), which are connected by lines (corresponding to putative flexible linker regions). Vesicular surface (with its coat proteins) is shown in black, and dynein and dynactin complexes as grey spheres (microtubule-BDs and microtubules are omitted for simplicity). Notice that the interaction of BICD2 with dynactin is direct, while that with dynein could be indirect. Stippled arrows indicate putative interactions of dynein and dynactin with each other and with the membrane coat; these interactions are not directly dependent on BICD2, but can be influenced by its presence in the complex.

Elucidation of the exact nature of the BICD2-associated cargoes would be necessary to test this prediction.

Studies in *Drosophila* oogenesis have shown that the genetic pathway involving Bic-D and cytoplasmic dynein–dynactin also includes Lis1 (Swan *et al*., 1999). Lis1 is a highly conserved protein, which was shown to have a function in dynein-mediated nuclear migration in filamentous fungi and to be essential for neuronal migration during brain development (for review see Vallee *et al*., 2001). Similar to BICD2, mammalian Lis1 co-precipitates both with the dynein and dynactin complexes, is partially localized to microtubule plus ends and is suggested to play a role in dynein function. We examined whether murine Lis1 interacts with BICD2 or the components of the dynactin complex described above using the yeast two-hybrid assay, but failed to show a positive reaction (data not shown). In addition, we could not show co-precipitation between BICD2 and GFP–Lis1 in overexpressing COS-1 cells (data not shown), indicating that BICD2 and Lis1 do not interact directly. Therefore, the respective roles of these proteins in dynein function await further analysis.

The membrane association of BICD2, described in this study, is a novel finding. It is supported by the high-speed fractionation and immunocytochemistry results (light microscopy and electron microscopy). The BFA studies suggest that BICD2 could be part of the peripheral coat of membranes. These data could be pertinent to the possible involvement of *D.melanogaster* Bic-D in microtubule-dependent mRNA transport (for discussion see Mach and Lehmann, 1997). Intracellular structures involved in mRNA localization, such as the *D.melanogaster* 'sponge body' and *Xenopus* mitochondrial cloud, contain abundant membranous components (Wilsch-Brauninger *et al*., 1997). An attractive possibility is that mRNA transport in early development and vesicular trafficking in cultured cells represent different aspects of essentially similar molecular mechanisms.

Materials and methods

Mammalian expression constructs

Full-length mouse BICD2 cDNA (ATCC 1364234) was sequenced on both strands (DDBJ/EMBL/GenBank accession No. AJ250106). The mammalian expression vectors pEGFP-C1 and -C2 (Clontech) were used to construct plasmids for the expression of full-length and truncated forms of mouse BICD2. Constructs for expressing GFP- and myc-tagged dynamitin and p150^{Glued} were a kind gift from Dr T.Schroer.

GST–BICD2 constructs and antibodies

For BICD2 antibody production, GST fusion proteins were made, purified and injected as described (Hoogenraad *et al*., 2000). Affinity purification of the antibodies was performed using standard methods (Spector *et al*., 1998). Monoclonal anti-Arp1 antiserum 45A (a kind gift from Dr T.Schroer) has been described (Schafer *et al*., 1994). Other antibodies, e.g. polyclonal anti-GFP antiserum (Clontech), monoclonal anti-γ-adaptin antibodies (Sigma), monoclonal anti-p115 and anti-p150^{Glued} antibodies (Transduction Laboratories), monoclonal anti-transferrin receptor and anti-myc antibodies (Boehringer) and monoclonal anti-intermediate chain dynein antibodies (IC74; Chemicon), were commercially acquired.

DNA transfections and immunofluorescence

COS-1 cells were transfected by the DEAE–dextran method as described (Hoogenraad *et al*., 2000), and HeLa cells were transfected with Superfect (Qiagen). BFA was purchased from Molecular Probes and nocodazole from Sigma. For immunofluorescence experiments, transfected cells were grown in Lab-Tek chambers slides (Nunc) for 18 or 40 h after transfection. Cells were fixed with 2% paraformaldehyde for 20 min at 20°C or with 100% methanol/1 mM EGTA for 10 min at –20°C, followed directly by a 2% paraformaldehyde fixation for 20 min at 20°C. Subsequent incubation steps were performed as described earlier (Hoogenraad *et al*., 2000). Polyclonal anti-BICD2 antibodies were used in a dilution of 1:300 and various monoclonal antibodies in a dilution of 1:100. Secondary antibodies used were fluorescein isothiocyanate (FITC)-conjugated goat anti-rabbit antibodies (Nordic Laboratories; 1:100), rhodamine-labelled sheep anti-mouse antibodies (Boehringer Mannheim; 1:25), Alexa 594-conjugated goat anti-rabbit antibodies (Molecular Probes; 1:500) and Alexa 350-conjugated sheep anti-mouse antibodies (Molecular Probes; 1:250). Slides were analysed with a Leica DMRBE microscope, equipped with a Hamamatsu CCD camera (C4880), or with a Zeiss confocal laser scanning microscope (LSM510). In the latter case, optical sections of 0.7–0.9 μm were taken.

Immunoelectron microscopy

The subcellular distribution of BICD2 was analysed by immunoelectron microscopy on ultrathin frozen sections, as plastic embedding was found to abolish antigen recognition by #2293 and #2298 antisera. COS cells were fixed with 3% paraformaldehyde for 1 h and scraped from the dish. Cell pellets were embedded in 10% gelatin and post-fixed in 3% paraformaldehyde for 24 h. Sectioning, immunolabelling and staining were performed as described before (Willemsen *et al*., 1987). Sections were examined in a Philips CM100 electron microscope at 80 kV.

Immunoprecipitations and western blot analysis

Immunoprecipitations were carried out using total protein extracts, prepared from HeLa cells or (transfected) COS-1 cells. Cells were lysed in buffer containing 25 mM Tris–HCl pH 8.0, 50 mM NaCl, 0.5% Triton X-100 and protease inhibitors (Boehringer), and incubated at 4°C for 30 min to depolymerize microtubules. All subsequent steps were performed as described (Hoogenraad *et al*., 2000). Anti-BICD2 antibodies were diluted 1:200 for immunoprecipitation and 1:2000 for western blotting, polyclonal anti-GFP and anti-CLIP-170 antibodies (Hoogenraad *et al*., 2000) were diluted 1:1000 for western blotting, and various monoclonal antibodies were diluted 1:100 for immunoprecipitation and 1:500 for western blotting.

For the immunodetection of BICD2 by western blotting, total protein extract was prepared from mock-transfected or BICD2-transfected COS-1 cells by homogenization in phosphate-buffered saline (PBS)/1% Triton X-100, in the presence of protease inhibitors. For fractionation experiments, COS-1 cells were homogenized in a sucrose buffer (10 mM HEPES pH 7.4, 0.25 M sucrose, 1 mM EDTA) using a glass homogenizer. A post-nuclear supernatant was recovered after centrifugation at 1000 *g*. Samples were subsequently centrifuged at 100 000 *g*, and pellet and high-speed supernatant were collected.

In-gel digestion of proteins

For the mass spectrometry identification of proteins co-precipitating with BICD2 antiserum, one flask (150 cm^2) of confluent HeLa cells was harvested and incubated with antibodies, as described above. Proteins were visualized with Coomassie Blue after SDS–PAGE (see Figure 1D) and the major bands were cut out. Excised, diced protein gel bands were washed, reduced and *S*-alkylated essentially as described (Wilm *et al*., 1996). A sufficient volume of 2 ng/µl trypsin (modified sequencing grade; Promega, Madison, WI) in 5 mM NH_4HCO_3 was added to cover the gel pieces and digestion performed overnight at 32°C in an incubator. The digests were then acidified by the addition of a 1/10 vol. of 2% trifluoroacetic acid prior to MALDI analysis

Peptide mass mapping by MALDI

A Reflex III MALDI time-of-flight mass spectrometer (Bruker Daltonik GmbH, Bremen, Germany), equipped with a nitrogen laser and a Scout-384 probe, was used to obtain positive ion mass spectra of digested protein with pulsed ion extraction in reflectron mode. An accelerating voltage of 26 kV was used with detector bias gating set to 2 kV and a mass cut-off of 650 *m/z*. Thin-layer matrix surfaces of α-cyano-4-hydroxycinnamic acid mixed with nitrocellulose were prepared as described (Shevchenko *et al*., 1996). An aliquot (0.4 µl) of acidified digestion supernatant was deposited onto the thin layer and allowed to dry prior to rinsing with water.

Peptide mass fingerprints thus obtained were searched against the non-redundant protein database placed in the public domain by the National Centre for Biotechnology Information (NCBI) using the program MS-FIT (Regents of the University of California).

Nanospray tandem mass spectrometry

Remaining digestion supernatant was loaded onto a 2 × 0.8 mm C18 microcolumn (LC Packings, Amsterdam, The Netherlands), washed and step eluted with 60% methanol, 0.1% formic acid directly into an Econo12 nanospray needle (New Objective Inc., Cambridge, MA). Nanospray mass spectra were acquired on an LCQ 'classic' quadrupole ion trap mass spectrometer (ThermoQuest Corporation, Austin, TX) equipped with a nanospray source (Protana, Odense, Denmark) operated at a spray voltage of 800 V and a capillary temperature of 150°C. Tandem (MS^2) mass spectra were acquired at a collision energy of 30% and a parent ion isolation width of 3 Da. Proteins were identified using the program SEQUEST (ThermoQuest Corporation, Austin, TX) to search tandem mass spectra against the NCBI non-redundant protein database.

Yeast two-hybrid analysis

The yeast two-hybrid analysis was performed as described previously (Wolthuis *et al*., 1996). Different mouse BICD2 fragments were linked to the GAL4 DNA-BD in the pPC97 yeast two-hybrid vector and to the GAL4 AD in the pPC86 yeast two-hybrid vector. Dynamitin and $p150^{Glued}$ cDNA fragments were generated by PCR, using the corresponding full-length cDNAs as templates. Arp1 and p24 cDNAs were generated by PCR, using total mouse brain cDNA as a template. Fragments were subcloned into pPC97. Production of the yeast fusion proteins of correct size was verified by western blotting, using antibodies against GAL4 DNA-BD and GAL4 AD and according to the protocol of the manufacturer (Clontech). β-galactosidase activity measurements (expressed in arbitrary units) were performed in triplicate from two independent experiments, as described previously (Ausubel *et al*., 1997).

Acknowledgements

We would like to thank Dr T.Schroer for the p50 and $p150^{Glued}$-encoding plasmids and the anti-Arp1 antibodies, Yvonne Krom and Arjan Theil for technical assistance, and Ruud Koppenol for photography. This research was supported by grants from the NWO (GB-MW 903-68-361) and SLW (805.33.310). N.G. was supported by the Royal Dutch Academy of Sciences (KNAW).

References

Ausubel,F.M., Brent,R., Kingston,R.E., Moore,D.D., Seidman,J.G., Smith,J.A. and Struhl,K. (1997) *Current Protocols in Molecular Biology*. John Wiley & Sons, Inc., New York, NY.

Baens,M. and Marynen,P. (1997) A human homologue (BICD1) of the *Drosophila* bicaudal-D gene. *Genomics*, **45**, 601–606.

Burkhardt,J.K., Echeverri,C.J., Nilsson,T. and Vallee,R.B. (1997) Overexpression of the dynamitin (p50) subunit of the dynactin complex disrupts dynein-dependent maintenance of membrane organelle distribution. *J. Cell Biol.*, **139**, 469–484.

Chardin,P. and McCormick,F. (1999) Brefeldin A: the advantage of being uncompetitive. *Cell*, **97**, 153–155.

Cole,N.B., Sciaky,N., Marotta,A., Song,J. and Lippincott-Schwartz,J. (1996) Golgi dispersal during microtubule disruption: regeneration of Golgi stacks at peripheral endoplasmic reticulum exit sites. *Mol. Biol. Cell*, **7**, 631–650.

Eckley,D.M., Gill,S.R., Melkonian,K.A., Bingham,J.B., Goodson,H.V., Heuser,J.E. and Schroer,T.A. (1999) Analysis of dynactin subcomplexes reveals a novel actin-related protein associated with the arp1 minifilament pointed end. *J. Cell Biol.*, **147**, 307–320.

Gill,S.R., Schroer,T.A., Szilak,I., Steuer,E.R., Sheetz,M.P. and Cleveland,D.W. (1991) Dynactin, a conserved, ubiquitously expressed component of an activator of vesicle motility mediated by cytoplasmic dynein. *J. Cell Biol.*, **115**, 1639–1650.

Harada,A., Takei,Y., Kanai,Y., Tanaka,Y., Nonaka,S. and Hirokawa,N. (1998) Golgi vesiculation and lysosome dispersion in cells lacking cytoplasmic dynein. *J. Cell Biol.*, **141**, 51–59.

Hoogenraad,C.C., Akhmanova,A., Grosveld,F., De Zeeuw,C.I. and Galjart,N. (2000) Functional analysis of CLIP-115 and its binding to microtubules. *J. Cell Sci.*, **113**, 2285–2297.

Karki,S. and Holzbaur,E.L. (1999) Cytoplasmic dynein and dynactin in cell division and intracellular transport. *Curr. Opin. Cell Biol.*, **11**, 45–53.

King,S.J. and Schroer,T.A. (2000) Dynactin increases the processivity of the cytoplasmic dynein motor. *Nature Cell Biol.*, **2**, 20–24.

Li,M., McGrail,M., Serr,M. and Hays,T.S. (1994) *Drosophila* cytoplasmic dynein, a microtubule motor that is asymmetrically localized in the oocyte. *J. Cell Biol.*, **126**, 1475–1494.

Mach,J.M. and Lehmann,R. (1997) An Egalitarian–Bicaudal-D complex is essential for oocyte specification and axis determination in *Drosophila*. *Genes Dev.*, **11**, 423–435.

McGrail,M., Gepner,J., Silvanovich,A., Ludmann,S., Serr,M. and Hays,T.S. (1995) Regulation of cytoplasmic dynein function *in vivo* by the *Drosophila* Glued complex. *J. Cell Biol.*, **131**, 411–425.

Muresan,V., Stankewich,M.C., Steffen,W., Morrow,J.S., Holzbaur,E.L. and Schnapp,B.J. (2001) Dynactin-dependent, dynein-driven vesicle transport in the absence of membrane proteins: a role for spectrin and acidic phospholipids. *Mol. Cell*, **7**, 173–183.

Nelson,D.S., Alvarez,C., Gao,Y.S., Garcia-Mata,R., Fialkowski,E. and Sztul,E. (1998) The membrane transport factor TAP/p115 cycles between the Golgi and earlier secretory compartments and contains distinct domains required for its localization and function. *J. Cell Biol.*, **143**, 319–331.

Oh,J. and Steward,R. (2001) Bicaudal-D is essential for egg chamber formation and cytoskeletal organization in *Drosophila* oogenesis. *Dev. Biol.*, **232**, 91–104.

Oh,J., Baksa,K. and Steward,R. (2000) Functional domains of the *Drosophila* Bicaudal-D protein. *Genetics*, **154**, 713–724.

Quintyne,N.J., Gill,S.R., Eckley,D.M., Crego,C.L., Compton,D.A. and Schroer,T.A. (1999) Dynactin is required for microtubule anchoring at centrosomes. *J. Cell Biol.*, **147**, 321–334.

Robinson,M.S. and Kreis,T.E. (1992) Recruitment of coat proteins onto Golgi membranes in intact and permeabilized cells: effects of brefeldin A and G protein activators. *Cell*, **69**, 129–138.

Saraste,J. and Kuismanen,E. (1984) Pre- and post-Golgi vacuoles operate in the transport of Semliki Forest virus membrane glycoproteins to the cell surface. *Cell*, **38**, 535–549.

Schafer,D.A., Gill,S.R., Cooper,J.A., Heuser,J.E. and Schroer,T.A. (1994) Ultrastructural analysis of the dynactin complex: an actin-related protein is a component of a filament that resembles F-actin. *J. Cell Biol.*, **126**, 403–412.

Shevchenko,A., Jensen,O.N., Podtelejnikov,A.V., Sagliocco,F., Wilm,M., Vorm,O., Mortensen,P., Boucherie,H. and Mann,M. (1996) Linking genome and proteome by mass spectrometry: large-

scale identification of yeast proteins from two dimensional gels. *Proc. Natl Acad. Sci. USA*, **93**, 14440–14445.

Spector,D.L., Goldman,R.D. and Leinwand,L.A. (1998) *Cells: A Laboratory Manual*. Cold Spring Harbor Laboratory Press, Cold Spring Harbor, NY.

Stuurman,N., Haner,M., Sasse,B., Hubner,W., Suter,B. and Aebi,U. (1999) Interactions between coiled-coil proteins: *Drosophila* lamin Dm0 binds to the Bicaudal-D protein. *Eur. J. Cell Biol.*, **78**, 278–287.

Suter,B. and Steward,R. (1991) Requirement for phosphorylation and localization of the Bicaudal-D protein in Drosophila oocyte differentiation. *Cell*, **67**, 917–926.

Suter,B., Romberg,L.M. and Steward,R. (1989) *Bicaudal-D*, a *Drosophila* gene involved in developmental asymmetry: localized transcript accumulation in ovaries and sequence similarity to myosin heavy chain tail domains. *Genes Dev.*, **3**, 1957–1968.

Swan,A. and Suter,B. (1996) Role of Bicaudal-D in patterning the Drosophila egg chamber in mid-oogenesis. *Development*, **122**, 3577–3586.

Swan,A., Nguyen,T. and Suter,B. (1999) *Drosophila* Lissencephaly-1 functions with Bic-D and dynein in oocyte determination and nuclear positioning. *Nature Cell Biol.*, **1**, 444–449.

Tai,A.W., Chuang,J.Z., Bode,C., Wolfrum,U. and Sung,C.H. (1999) Rhodopsin's carboxy-terminal cytoplasmic tail acts as a membrane receptor for cytoplasmic dynein by binding to the dynein light chain Tctex-1. *Cell*, **97**, 877–887.

Theurkauf,W.E., Alberts,B.M., Jan,Y.N. and Jongens,T.A. (1993) A central role for microtubules in the differentiation of *Drosophila* oocytes. *Development*, **118**, 1169–1180.

Vallee,R.B., Tai,C. and Faulkner,N.E. (2001) LIS1: cellular function of a disease-causing gene. *Trends Cell Biol.*, **11**, 155–160.

Vaughan,K.T. and Vallee,R.B. (1995) Cytoplasmic dynein binds dynactin through a direct interaction between the intermediate chains and p150Glued. *J. Cell Biol.*, **131**, 1507–1516.

Vaughan,K.T., Tynan,S.H., Faulkner,N.E., Echeverri,C.J. and Vallee,R.B. (1999) Colocalization of cytoplasmic dynein with dynactin and CLIP-170 at microtubule distal ends. *J. Cell Sci.*, **112**, 1437–1447.

Wharton,R.P. and Struhl,G. (1989) Structure of the *Drosophila* Bicaudal-D protein and its role in localizing the posterior determinant nanos. *Cell*, **59**, 881–892.

Willemsen,R., van Dongen,J.M., Ginns,E.I., Sips,H.J., Schram,A.W., Tager,J.M., Barranger,J.A. and Reuser,A.J. (1987) Ultrastructural localization of glucocerebrosidase in cultured Gaucher's disease fibroblasts by immunocytochemistry. *J. Neurol.*, **234**, 44–51.

Wilm,M., Shevchenko,A., Houthaeve,T., Breit,S., Schweigerer,L., Fotsis,T. and Mann,M. (1996) Femtomole sequencing of proteins from polyacrylamide gels by nano-electrospray mass spectrometry. *Nature*, **379**, 466–469.

Wilsch-Brauninger,M., Schwarz,H. and Nusslein-Volhard,C. (1997) A sponge-like structure involved in the association and transport of maternal products during *Drosophila* oogenesis. *J. Cell Biol.*, **139**, 817–829.

Wolthuis,R.M., Bauer,B., van't Veer,L.J., de Vries-Smits,A.M., Cool,R.H., Spaargaren,M., Wittinghofer,A., Burgering,B.M. and Bos,J.L. (1996) RalGDS-like factor (Rlf) is a novel Ras and Rap 1A-associating protein. *Oncogene*, **13**, 353–362.

Young,A., Dictenberg,J.B., Purohit,A., Tuft,R. and Doxsey,S.J. (2000) Cytoplasmic dynein-mediated assembly of pericentrin and γ tubulin onto centrosomes. *Mol. Biol. Cell*, **11**, 2047–2056.

Received January 4, 2001; revised May 31, 2001; accepted June 11, 2001